

Flow Visualization Study on the Effect of a Gurney Flap in a Low Reynolds Number Compressor Cascade

Roy Y. Myose,*

Wichita State University, Wichita, KS 67260-0044

Jan-Christopher Lietsche,[†] Dieter Scholz,[‡] Hartmut Zingel,[‡]
Hamburg University of Applied Sciences, Hamburg, Germany

Shigeo Hayashibara,[§]

Embry-Riddle Aeronautical University, Prescott, AZ 86301

and Ismael Heron[¶]

Eclipse Aviation Corporation, Albuquerque, NM 87106

The effect of a Gurney flap in a compressor cascade model at low Reynolds number was investigated using tuft flow visualization in a water table facility. Although small in scale, water tables have the advantage of low cost and the ease with which test conditions can be varied. In this experiment, tuft flow visualization was used to determine the outgoing flow angle for a NACA 65-(12)10 compressor cascade model with a solidity of 1.5 at a blade chord Reynolds number of 16,000. The baseline (no flap) results were found to be in good agreement compared to results in the literature for tests conducted at Reynolds number in the 250,000⁺ range. A second set of measurements were then taken for a Gurney flap with a height of 2% of the chord length attached to the trailing edge of the cascade blades. The results suggest that the Gurney flap energizes the flow and delays the stall at large incoming flow angles.

Nomenclature

c	= chord length
Re_c	= Reynolds number based on chord length, Uc/ν
U	= freestream velocity
y	= offset distance in the stagger direction
β_{in}	= incoming flow angle, between the in-flow direction and a line perpendicular to the stagger line
β_{out}	= outgoing flow angle, between the out-flow direction and a line perpendicular to the stagger line
λ	= stagger angle, between the chord line and a line perpendicular to the stagger line
ν	= kinematic viscosity
σ	= solidity of cascade, c/y

Introduction

The first century of heavier-than-air powered flight has been dominated by the desire to fly "faster, higher, and farther." Fulfilling this desire led to the development of the gas turbine driven turbojet. Since their introduction more than six decades ago, gas turbine driven engines have become quite powerful in terms of thrust produced¹ while achieving significant improvements in fuel efficiency² and reductions in maintenance costs³. Today, gas turbine driven turbofans and turboprops dominate the field of aero-propulsion for aircraft varying from "moderate" size general aviation planes to large passenger jets. This domination of gas turbine engines is true even in some "smaller" aircraft like Unmanned Aerial Vehicles (UAV) including the Air Force RQ-4A Global Hawk and HQ-9A Predator B. Since gas turbine engines are so prevalent in aviation, it is important to learn what affects their performance. Gas turbine

*Professor, Department of Aerospace Engineering, Associate Fellow AIAA.

[†]Student, Automotive and Aeronautical Engineering Department.

[‡]Professor, Automotive and Aeronautical Engineering Department.

[§]Assistant Professor, Department of Aerospace Engineering, Member AIAA.

[¶]Flight Test Engineer, Member AIAA.

driven engines are designed for, and can typically be operated at, optimum performance in medium to large size aircraft applications because their flight envelopes are so well defined. However, recent advances in UAV applications have pushed the flight envelope into the lesser known low Reynolds number flight regime.

A typical general aviation aircraft may involve wing chord Reynolds number on the order of 10^6 to 10^7 while large passenger aircraft might be in the 10^8 range.⁴ Recently, however, there has been a strong interest in very small reconnaissance vehicles called Micro Air Vehicles (MAV) which typically have a wing chord length on the order of 6 inches (0.15 m). MAV's involve chord Reynolds number on the order of 20,000 to 200,000, and very little aerodynamic data exists in this range.⁵ Similar issues exist in the gas turbine engine research area as well. A micro-scale engine (i.e., micro-fabricated gas turbine) for application on MAV involves design blade chord Reynolds numbers of about 20,000 or less.⁶ In addition to small-scale effects, extreme operating conditions on conventional gas turbine engines often result in low Reynolds numbers. The low-pressure turbine blades on UAV engines, which are in operation today, involve blade chord Reynolds numbers less than 25,000 under high-altitude operating conditions.⁷ However, currently existing data for turbomachinery blades only go as low as Reynolds numbers in the 40,000 range.^{8,9} Thus, there is a strong need to obtain data for turbomachinery blades at the low Reynolds number range.

Modern gas turbines oftentimes employ a multi-stage axial compressor where the pressure rise across each compressor stage is relatively small. Since compressor blades operate in an adverse pressure gradient environment, it is relatively easy to cause flow separation (i.e., stall). The consequences of compressor blade stall can simply be poor performance or, in the worst case scenario, significant engine damage.³ In order to prevent compressor blade stall, gas turbine engines are normally operated close to its design operating condition. This means that their performance and operating limits must be well defined. The flow behavior of compressor cascades is controlled by a number of different parameters which are shown in the left-hand illustration of figure 1. A compressor cascade consists of a series of blades offset by a distance y along the stagger line, which connects the leading edges of the blades. Non-dimensionalizing this distance by the chord length c then defines the solidity σ (i.e., $\sigma = c/y$). More densely packed blades have a large solidity value while loosely packed blades have a small solidity value. The directions for the incoming flow, outgoing flow, and blade chord line are all measured with respect to a line drawn perpendicular to the stagger line. Here, the incoming flow angle is β_{in} , the outgoing flow angle is β_{out} , and the stagger angle λ measures the direction of the blade chord line. The difference between the incoming flow angle β_{in} and the stagger angle λ is essentially the angle of attack. If the angle of attack ($\beta_{in} - \lambda$) is too large or too small (i.e., large negative value), then the flow will separate. However, the presence of nearby blades affects the flow which means that the solidity σ plays a role in determining the flow behavior.

The right-hand illustration of figure 1 shows the cascade flow behavior at a fixed solidity (σ) for varying flow conditions (β_{in} and λ). For a fixed stagger angle, an incoming flow angle which is too small leads to negative stall while an incoming flow angle which is too large leads to positive stall. It is interesting to note that changing the incoming flow angle near the design operating point (i.e., the interior of the λ curve) does not significantly affect the outgoing flow angle. Although the positive and negative stall "limits" are shown by the dashed lines in the figure, these "limits" are actually conditions corresponding to a 50% increase in the blade profile loss coefficient³ rather than the fully separated flow condition associated with stall in airfoil aerodynamics. Test results such as those shown in the right-hand illustration of figure 1 are available in the literature for the NACA 65 series compressor cascades at chord Reynolds numbers ranging from 245,000 to 445,000.¹⁰ Determining whether the cascade behaves in a similar manner at a much lower Reynolds number is one of the objectives of the present study.

Turning our attention to the low Reynolds number regime, the nature of the flow at low Reynolds numbers is predominantly laminar. Although the smaller skin friction drag associated with laminar flow is an advantage compared to turbulent flow, there is a strong tendency for the flow to separate at low Reynolds numbers. According to Byerley *et al.*¹¹, the use of Gurney flaps reduced the tendency of turbine cascades to stall, by forcing flow from a neighboring blade down onto the laminar separation bubble. The Gurney flap is a short flat plate oriented perpendicular to the flow at the trailing edge of the pressure side of the airfoil as shown in figure 2. Liebeck¹² and others¹³⁻¹⁶ have found that a properly scaled Gurney flap can increase the lift without an appreciable increase in the drag for two-dimensional airfoils as well as a variety of wing configurations. The Gurney flap basically causes the downstream flow to be turned (more than with the no-flap configuration) as illustrated in the side detail of figure 2. This leads to an increase in lift while the increase in drag is kept to a minimum as long as the Gurney flap remains inside the airfoil boundary layer.¹⁷ Although the effect of Gurney flaps on turbine cascades has been investigated by Byerley *et al.*¹¹, the authors are not aware of any such investigation for *compressor* cascades. Thus, the second objective of this study is to determine the effect of a Gurney flap on a compressor cascade.

Experimental Method

The experiment was conducted in the Wichita State University (WSU) water table facility. Water tables have been used in the past for cascade tests, especially as hydrodynamic flow analogies for compressible flow visualization of transonic and supersonic turbine cascades.¹⁸ However, the lack of a quantitative measurement technique at low speeds has precluded the use of water tables as a tool for testing subsonic compressors and turbines in the past. Hayashibara *et al.*^{19,20} employed a simple hydrogen bubble time line technique to obtain detailed boundary layer velocity profile data for a compressor cascade model in the WSU water table facility. The present experiment complements their work by employing tuft flow visualization to determine the outgoing flow angle on a similar cascade model.

The WSU water table is shown schematically in figure 3. This water table is a closed return-type facility consisting of a settling chamber, a 3½ ft (1.1 m) wide by 6 ft (1.8 m) long test section, a return tank, and an impeller pump driven by a 0.75 hp DC motor. The facility contains a total water volume of about 125 gallons (473 litres). Supercritical high-speed flows, which are analogous to supersonic compressible flows, can be obtained by lowering the sluice gate to increase the stagnation water level in the settling chamber. However, the sluice gate shown in the figure was not used in this experiment since subcritical low speed flows were desired. Under subcritical conditions, the test section flow speed can be varied in range from 0.05 to 0.2 ft/s (0.015 - 0.06 m/s) by adjusting the bypass valve on the pipe parallel to the constant speed impeller pump. The current tests were conducted at a speed of 0.17 ft/s (0.052 m/s) on 1 ft (0.305 m) chord length cascade blades which resulted in a chord Reynolds number of about 16,000.

The cascade model tested in the present experiment is the NACA 65-(12)10 profile blade. This particular profile has a design lift coefficient of $C_L = 1.2$ (i.e., 12) and a maximum thickness of 10% of chord length, which is the reason for the (12)10 designation. Ten identical 1 ft (0.305 m) long NACA 65-(12)10 profile blades were constructed from styrofoam, painted black, and sanded down to a smooth finish. Five of the blades were left in the clean (baseline) configuration while 0.25 inch (0.0064 m) high Gurney flaps were attached on the remaining five blades. The set-up of the cascade model in the water table is shown schematically in the left-hand illustration of figure 4. All the tests were conducted at a solidity of $\sigma = 1.5$ which meant that the offset distance was $y = 8$ inches (0.203 m).

A pair of bolts were glued to each blade at the quarter and half chord locations. The blades were then attached to a pair of wooden supports as shown in the right-hand illustration of figure 5. The blades were free to pivot to any angle since the bolts were loosely attached to the supports. The desired incoming flow angle β_{in} could be obtained by rotating both wooden supports (i.e., about the lower water table side wall as illustrated in figure 4). The desired stagger angle λ could be obtained by moving one support relative to the other so that the blades rotated about the half chord pivot location.

Although five blades were used in the tests, the top and bottom blades were employed as part of the false walls in order to properly orient the general flow direction (see left-hand illustration of figure 4). Setting the angle on the downstream false walls involved an iterative technique where the out-flow direction was visually measured for different false wall angles until the false wall angle matched the out-flow direction. There were no attempts to remove the boundary layer which developed along the upstream and downstream false walls since they were likely to be relatively small in these small scale tests.

Six darkly colored 0.004 inch (0.000102 m) diameter threads, commercially available for sewing, were employed as tufts for flow visualization. When placed in the flow, the tuft aligns in the flow direction (i.e., orients itself to minimize drag) while the flow is left undisturbed due to their small diameter. These tufts were located in the lower, middle, and upper part of the channel (each offset 2 inches or 0.05 m apart) in-between the middle three cascade blades as shown schematically in the right-hand illustration of figure 4. Each tuft was attached to a black-colored support which is visible in the right-hand photograph of figure 5. The black-colored support is parallel to the stagger line, but offset from the trailing edge in the downstream direction by a distance of 1/8th of a chord length (1.5 inches or 0.038 m). Although each tuft was 6 inches (0.15 m) long, about one-third of the length was used in "free-falling" off the black-colored support so the effective length of the tufts in the water was about 4 inches (0.10 m). In order to determine the tuft angle, a reference grid pattern of 1 inch (0.0254 m) squares was attached below the transparent floor of the water table. The "horizontal" lines in this grid pattern are parallel to the water table side wall and therefore parallel to the in-flow direction. This grid pattern along with the 2 mega-pixel resolution digital camera (Concord Eye-Q Go 2000) and supporting tripod are visible in figure 5. The image plane of the digital camera was oriented parallel to the water table surface to minimize parallax error. Based on data analysis for a random sample of captured images, the reference grid lines in the captured images were found to be perpendicular within ± 0.5 degrees.

A VisualBASIC[®] based software program was written to assist in the data analysis of the captured flow visualization images. Figure 6 shows the schematic of the image capture and data analysis process. Three major pieces were required to perform the data analysis. First, the stagger angle λ and the incoming flow angle β_{in} must be specified

based on the experimental set-up. Second, the "horizontal" reference grid line direction must be defined in order to determine the in-flow direction. Finally, the tuft flow direction must be determined. Both the "horizontal" reference line and tuft flow direction were determined in terms of pixel values by the VisualBASIC[®] software program. This information was then converted into angle information by an Excel[®] spreadsheet program. Figure 7 shows a sample window screen from the VisualBASIC[®] software program along with one of the captured images. In this figure, the flow generally moves from the bottom of the image to the top. The rear third of the upper, middle, and (trailing edge of) lower cascade blades are visible in the bottom left, bottom center, and bottom right part of the image, respectively. The "clickable" buttons in the lower part of the window screen are file input and output commands. When the "mouse" cursor is moved within the area of the captured image, the pixel value of the current cursor position is displayed. If the "mouse" button is then "clicked," a reference point is drawn in the captured image and the pixel value for that location is specified as the starting point for the line. After moving the "mouse" cursor to a new location and "clicking" once more, a line is drawn connecting the two points and the pixel value of the new location is displayed as the ending point of the line. A faint yellow line in figure 7 highlights the location of tuft #1 using this process. Finally, the pixel values for the start and end points of the line can be output to a file before the process is repeated once again for another line. Thus, the software program can provide angle information from the captured images based on user input. To reduce the likelihood of user input error, each line was defined four times and the average of the four was used for the final angle value.

Results and Discussion

The test matrix consisted of the baseline (clean) cascade and the case with a 2% height Gurney flap for stagger angles varying from $\lambda = 20$ to 50 in 5 degree increments. A typical data set consisted of three to five different incoming flow angles (β_{in}). The particular in-flow angles chosen depended upon the stall limit data which were available in the literature (for much higher test Reynolds numbers). For each flow condition (λ and β_{in}), three test runs were conducted (i.e., three images were captured) and data from these three runs were averaged for the results which follow. Measurements of the outgoing flow angle β_{out} were obtained for each of the six tuft locations shown earlier in figure 4. Strictly speaking, these tufts alone would not be able to specify the exact out-flow direction due to the limited number of spatial positions in the measurements. Nevertheless, the average of the six tufts provide a good sense of the general out-flow direction. It should be noted that the data for tuft #1 is the same as tuft #4 since they are both located near the upper part of a blade. Similarly, tuft #2 provides the same data as tuft #5 and tuft #3 is analogous to tuft #6. Consequently, the average of the results for tuft #1 and #4 will be referred to as those for the upper (suction) surface, tuft #2 and #5 as data for the middle of the channel, and tuft #3 and #6 as data for the lower (pressure) surface, respectively.

Figure 8 presents the results for the baseline (clean) configuration. The dashed-line curve presents the average of the six tufts from the present experiment. The solid-line curve presents data from the literature³ for the same NACA 65-(12)10 cascade, but at a much higher Reynolds number. The present results for test Reynolds number of 16,000 are in good agreement (within ± 2 degrees) compared to those in the literature taken at test Reynolds number above 250,000. In general, the present results (dashed-line) are slightly above those from the literature (solid-line) with the only exception being the results for $\lambda = 40$ and 45 which show the dashed and solid-line curves extremely close to each other. It should be noted that there were no attempts to determine the stall limits since it was not possible to determine the blade profile loss coefficient based on tuft flow visualization. However, the extent of the solid-line curves in figure 8 provides a rough representation of the stall limits at the higher Reynolds number based on results presented in the literature.

Figure 8 also shows the measured out-flow angles over the upper surface (triangles), middle of the channel (squares), and lower surface (diamonds). Results at stagger angles of $\lambda = 20$ and 40 degrees are shown with open symbols while the results at stagger angles of $\lambda = 30$ and 50 degrees are shown with filled symbols. Although the average results for the ($\lambda=30, \beta_{in}=35$) and ($\lambda=40, \beta_{in}=42$) baseline cases and the ($\lambda=30, \beta_{in}=30$) Gurney flap case were determined, the detailed data for these cases were unfortunately lost before the upper/middle/lower tuft results could be calculated. It is quite evident that the upper surface tuft has a noticeably lower out-flow angle (by about 2 to 8 degrees) compared to the middle and lower surface tufts when the flow condition (i.e., λ and β_{in}) is near the operating condition for this cascade. On the other hand, all of the tufts are at nearly the same out-flow angle when the cascade is operated at the positive and negative stall limits. At first glance, the results at ($\lambda = 20, \beta_{in} = 30$) would not appear to fit this trend. However, the negative stall limits occur at $\beta_{in} < 30$ degrees - i.e., the negative stall results were not obtained (or shown) in the literature for this particular stagger angle.

Based on these upper/middle/lower tuft results, the envisioned cascade flow behavior for the baseline (clean) configuration is shown in figure 9. When the cascade is driven at the operating condition (referred to as the unstalled case in the figure), the upper surface tuft substantially turns the flow. This would correspond to the high lift situation in traditional airfoil aerodynamics terms. On the other hand, the flow turning capability is diminished when the cascade blade is driven at (or beyond) the negative or positive stall limits. Since the general out-flow angle increases slightly with increasing in-flow angle, tuft #2, 3, 5, and 6 are represented with slightly larger out-flow angles (i.e., arrows are slightly above the dashed-lines) for the positive stall case shown in figure 9. Similar out-flow angles are shown for the unstalled case in figure 9 since the square and diamond symbols are located above the average in the corresponding situation in figure 8.

Figure 10 shows tuft flow visualization for the operating condition situation ($\lambda = 30$, $\beta_{in} = 45$). The left-hand image shows the baseline (clean) configuration while the right-hand image shows the 2% height Gurney flap case. In the right-hand image, the Gurney flap is visible in the upper-most cascade blade, but are hidden from view in the other two blades due to the presence of the tuft supports along the downstream direction. At this unstalled, operating condition situation, the tuft over the upper surface is turned substantially more than the middle and lower surface tufts. Although somewhat difficult to see (from these side-by-side images), the Gurney flap turns all of the tufts compared to the baseline (clean) configuration.

Figure 11 presents the results for the cascade with Gurney flap configuration. For reference purposes, the solid-line curve in the figure presents the same NACA 65-(12)10 cascade results from the literature³ for the baseline (clean) configuration at a much higher Reynolds number. The dashed-line curve presents the average of the six tufts from the present experiment for the Gurney flap configuration. All of the Gurney flap results have an out-flow angle which is 2 to 5 degrees smaller than the comparable baseline (clean) configuration data from the literature. It should be noted that the baseline (clean) configuration results from the present experiment generally had out-flow angles which were a few degrees greater than the results from the literature (see figure 8).

Also shown in figure 11 are the measured out-flow angles over the upper surface (triangles), middle of the channel (squares), and lower surface (diamonds). Compared to the baseline (clean) configuration, the Gurney flap has turned the flow to a smaller out-flow angle everywhere (upper, middle, and lower regions). With the exception of the ($\lambda = 40$, $\beta_{in} = 42$) and ($\lambda = 50$, $\beta_{in} = 65$) cases, the upper surface out-flow angle is considerably less than the out-flow angles at the middle and lower regions. This is true even for in-flow angles associated with positive stall in the baseline (clean) configuration. This suggests that the Gurney flap helps to energize the flow and delays the stall at large in-flow angles.

Conclusions

The effect of a Gurney flap in a compressor cascade model at low Reynolds number was investigated using tuft flow visualization in a water table facility. The NACA 65-(12)10 compressor cascade with a solidity of 1.5 was tested at a blade chord Reynolds number of 16,000. A computer assisted data analysis software program was used to determine the flow direction based on digital images of the tuft flow visualization. The baseline (no flap) results were found to be in good agreement compared to results in the literature for tests conducted at Reynolds number in the 250,000⁺ range. A second set of measurements were then taken for a Gurney flap with a height of 2% of the chord length attached to the trailing edge of the cascade blades. The results suggest that the Gurney flap energizes the flow and delays the stall at large incoming flow angles. The present results provide information about the operating conditions which are suitable for this compressor cascade with and without Gurney flaps. However, tuft flow visualization is unable to provide any information about the associated losses for this compressor cascade. Current plans are to report on loss information based on boundary layer profile measurements for this compressor cascade in future papers.

Acknowledgements

The authors acknowledge the assistance of Gordon Sim who performed some of the data analysis.

References

- ¹Otis, C.E., 1991, *Aircraft Gas Turbine Powerplants*, IAP, Inc., Casper.
- ²Shevell, R.S., 1983, *Fundamentals of Flight*, Prentice-Hall, New Jersey.
- ³Hill, P.G. and Peterson, C.R., 1992, *Mechanics and Thermodynamics of Propulsion*, McGraw-Hill, N.Y.

- ⁴Pelletier, A. and Mueller, T.J., 1999, "Low Reynolds Number Aerodynamics of Low-Aspect-Ratio Wings," AIAA 99-3182.
- ⁵Pelletier, A. and Mueller, T.J., 2000, "Low Reynolds Number Aerodynamics of Low-Aspect-Ratio, Thin/Flat/Cambered Wings," *Journal of Aircraft*, Vol.37, No.5, pp.825-832.
- ⁶Jacobson, S.A., 1998, "Aerothermal Challenges in the Design of a Microfabricated Gas Turbine Engine," AIAA 98-2545.
- ⁷Bons, J.P., Sondergaard, R., and Rivir, R.B., 1999, "Control of Low-Pressure Turbine Separation Using Vortex Generator Jets," AIAA 99-0367.
- ⁸Lake, J.P., King, P.I., and Rivir, R.B., 1999, "Reduction of Separation Losses on a Turbine Blade with Low Reynolds Number," AIAA 99-0242.
- ⁹Lake, J.P., King, P.I., and Rivir, R.B., 2000, "Low Reynolds Number Loss Reduction on Turbine Blades with Dimples and V-grooves," AIAA 2000-0738.
- ¹⁰Emery, J.C., Herrig, L.J., Erwin, J.R., and Felix, A.R., 1958, "Systematic Two-dimensional Cascade Tests of NACA 65-series Blades at Low Speeds," NACA Report 1368.
- ¹¹Byerley, A.R., Sormer, O., Baughn, J.W., Simon, T.W., Van Treuren, K.W., and List, J., 2003, "Using Gurney Flaps to Control Laminar Separation on Linear Cascade Blades," *Journal of Turbomachinery*, Vol. 125, No. 1, pp. 114-120.
- ¹²Liebeck, R., 1978, "Design of Subsonic Airfoils," *Journal of Aircraft*, Vol. 15, No. 9, pp.547-561.
- ¹³van Dam, C.P., Yen, D.T., and Vijgen, P.M.H.W., "Gurney Flap Experiments on Airfoils and Wings," *Journal of Aircraft*, Vol. 36, No. 2, pp. 484-486.
- ¹⁴Myose, R.Y., Papadakis, M., and Heron, I., 1998, "Gurney Flap Experiments on Airfoils, Wings, and Reflection Plane Model," *Journal of Aircraft*, Vol. 35, No. 2, pp. 206-211.
- ¹⁵Myose, R., Heron, I., and Papadakis, M., 1997, "The Post-stall Effect of Gurney Flaps on NACA 0011 Airfoil," *SAE Transactions Journal of Aerospace*, Vol. 105, p. 173-178 (also SAE paper 96-1316).
- ¹⁶Brown, L. and Filippone, A., September 2003, "Aerofoil at Low Speeds with Gurney Flaps," *Aeronautical Journal*, Vol. 107, No. 1075, pp. 539-546.
- ¹⁷Giguere, P., Dumas, G., and Lemay, J., 1997, "Gurney Flap Scaling for Optimum Lift-to-Drag Ratio," *AIAA Journal*, Vol. 35, No. 12, pp. 1888-1890.
- ¹⁸Cicatelli, G. and Sieverding, C.H., 1996, "A Review of the Research on Unsteady Turbine Blade Wake Characteristics," *AGARD Conference Proceedings CP-571*.
- ¹⁹Hayashibara, S., Myose, R.Y., Heron, I., and Miller, L.S., "Development of a Low Cost Cascade Aerodynamics Test Facility using a Simple Flow Visualization Velocimetry Technique," SAE paper 2002-01-1543.
- ²⁰Hayashibara, S., Myose, R.Y., and Davies, M.R.D., "Development of a Water Table Cascade Aerodynamics Test Facility using a Simple Flow Visualization and Image Processing Technique," AIAA paper 2003-4136.

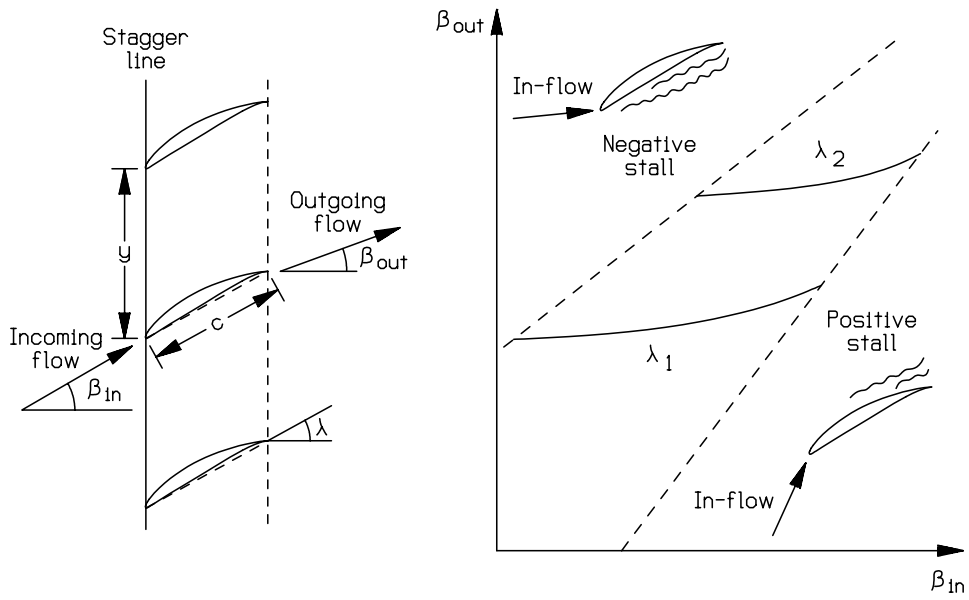


Figure 1 – Compressor cascade geometry (left) and stall limit results (right).³

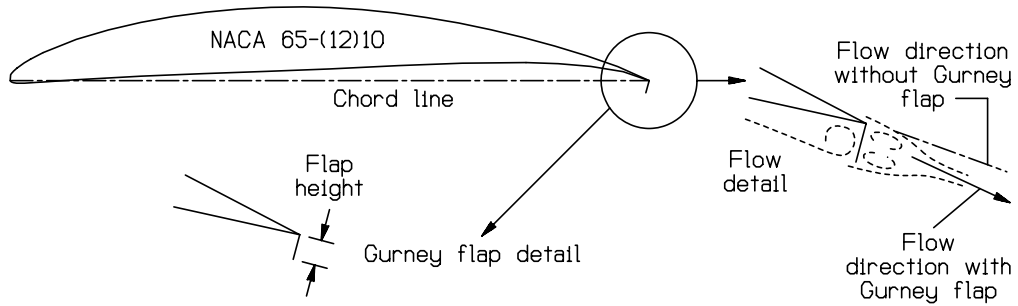


Figure 2 – Gurney flap.

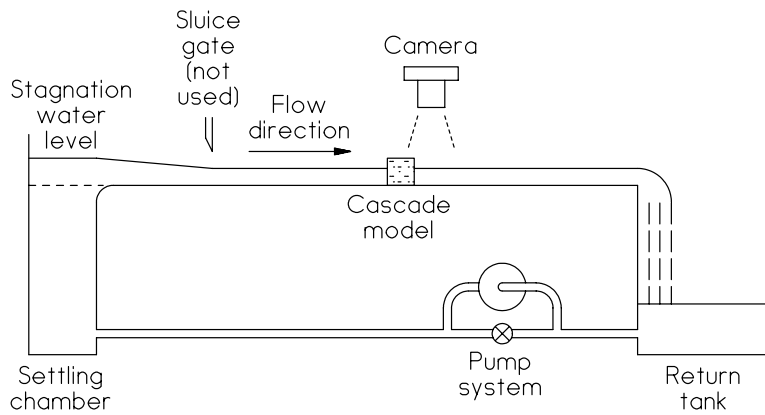


Figure 3 – Schematic of water table facility.

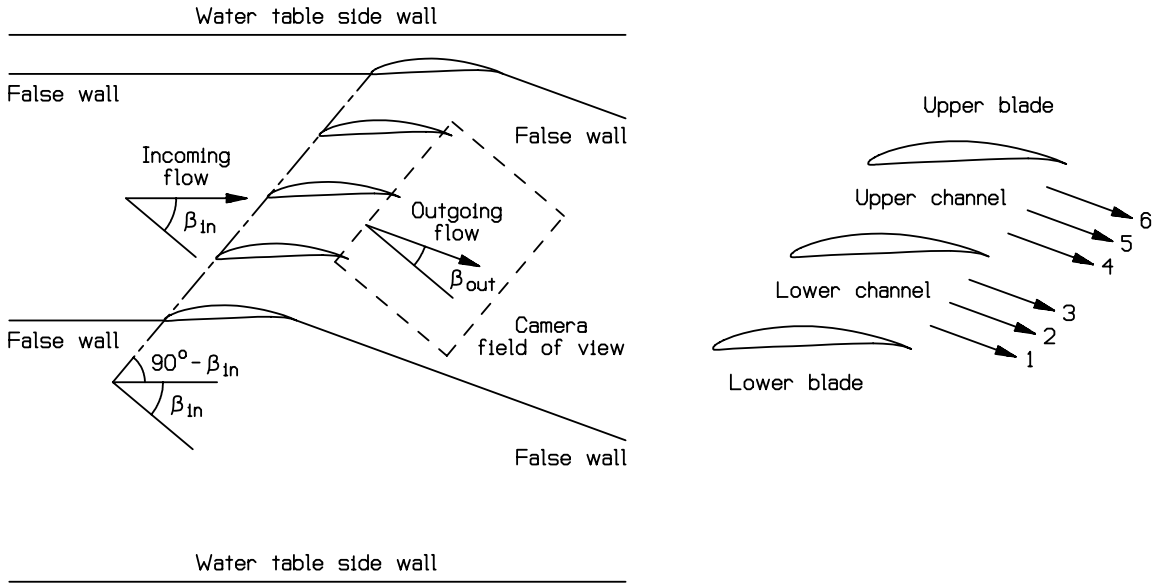


Figure 4 – Water table cascade set-up (left) and tuft flow visualization configuration (right).



Figure 5 – Water table cascade set-up with grid lines, view from downstream (left) & view from upper blade (right).

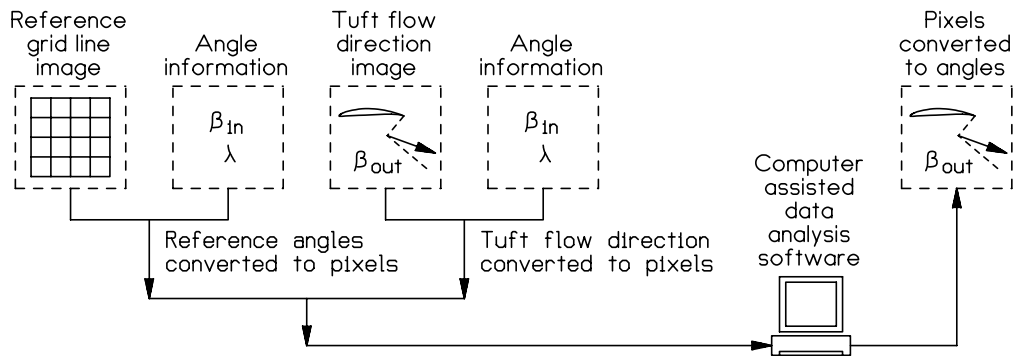


Figure 6 – Schematic of data analysis process.



Figure 7 – Computer assisted data analysis window screen shown with a yellow line highlighting angle for tuft #1.

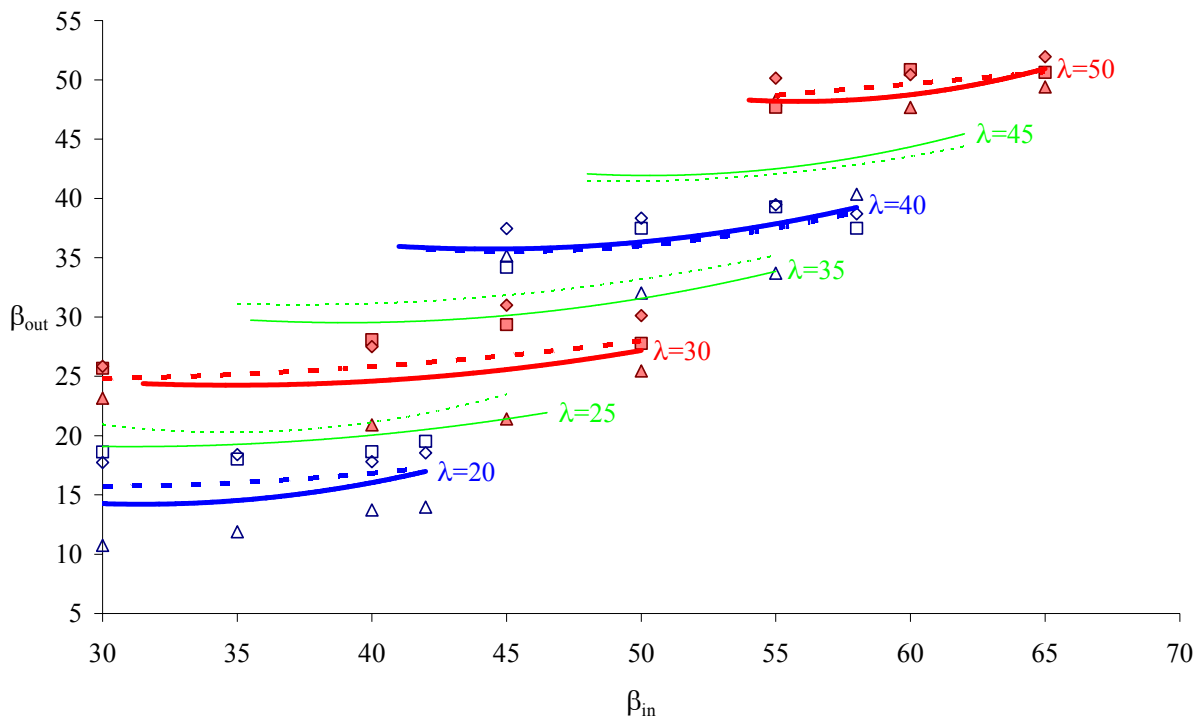


Figure 8 – Baseline results (without Gurney flap): — data from Hill & Peterson³, - - - average of tufts 1-6, Δ tuft near upper (suction) surface (average of tuft 1 & 4), \square tuft at middle of channel (average of tuft 2 & 5), and \diamond tuft near lower (pressure) surface (average of tuft 3 & 6) with open symbols for $\lambda=20$ & 40 and filled symbols for $\lambda=30$ & 50. (See figure 4 for explanation of tuft location numbers.)

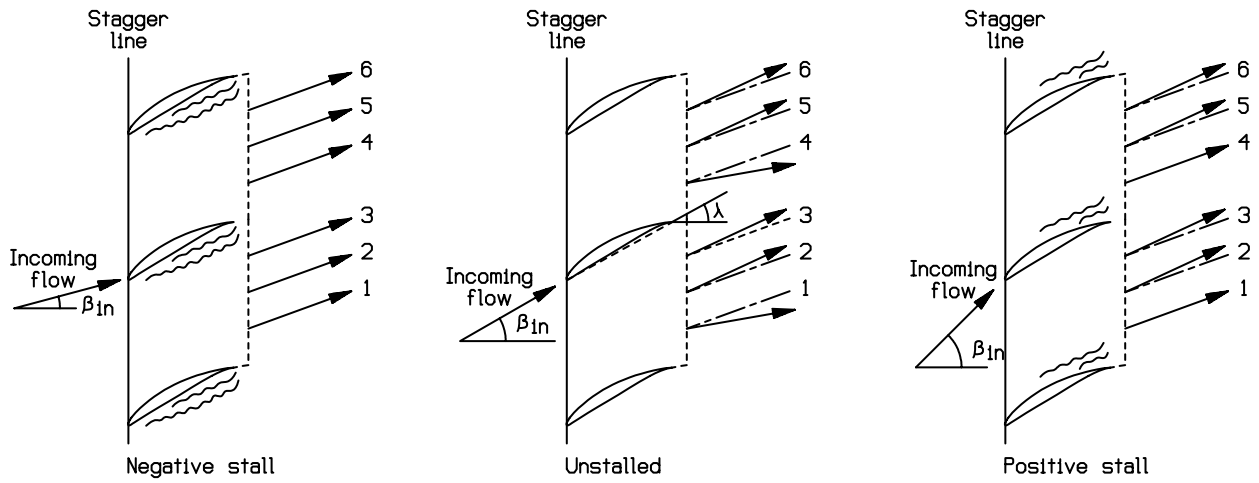


Figure 9 – Envisioned cascade flow behavior.

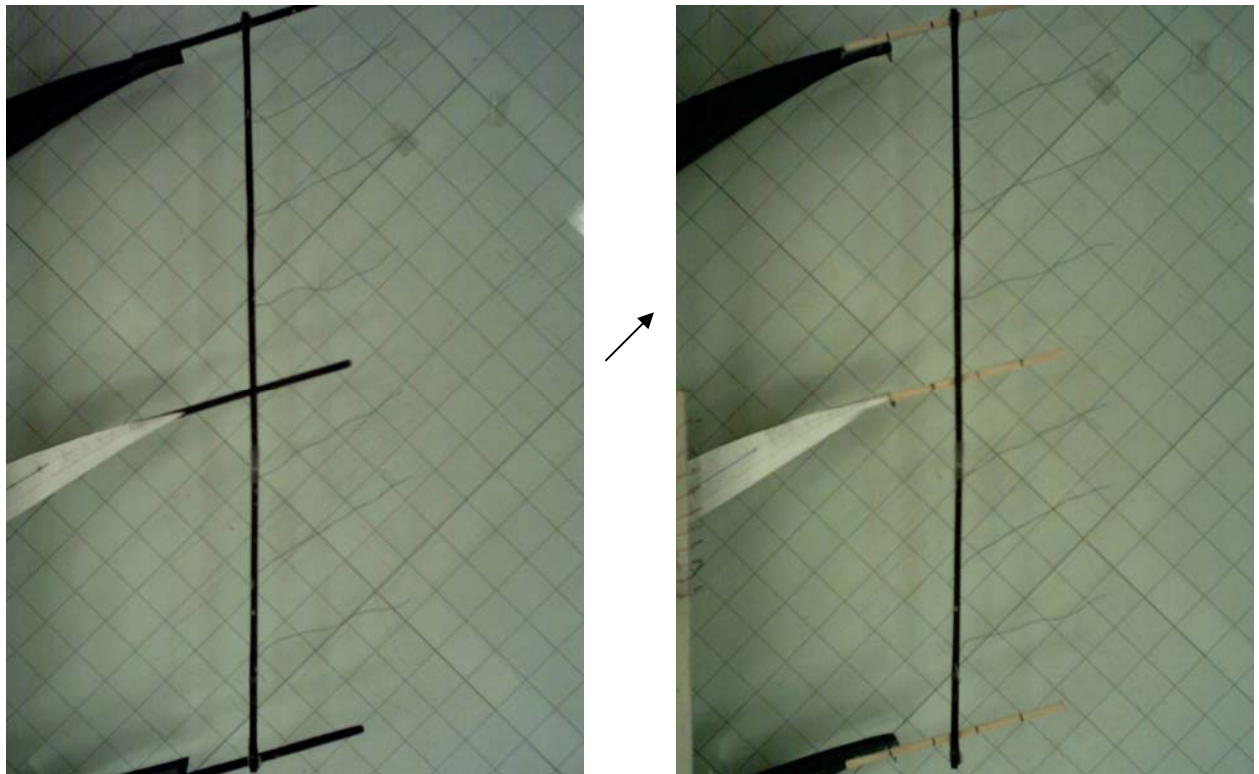


Figure 10 – Captured tuft flow visualization images at $\beta_{in}=45$ and $\lambda=30$: without (left) and with Gurney flap (right). The incoming flow direction (β_{in}) is indicated by the arrow which is shown in between the two images.

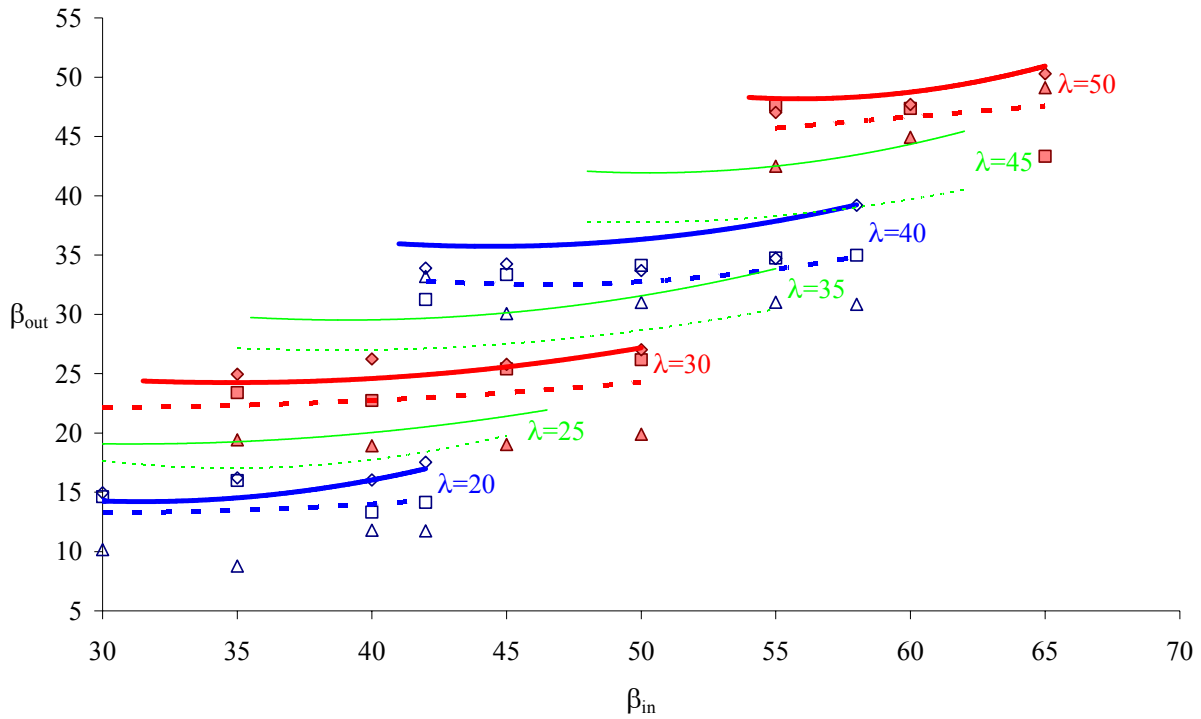


Figure 11 – Cascade with Gurney flap results: — — — average of tufts 1-6, Δ tuft near upper (suction) surface (average of tuft 1 & 4), \square tuft at middle of channel (average of tuft 2 & 5), and \diamond tuft near lower (pressure) surface (average of tuft 3 & 6) with open symbols for $\lambda=20$ & 40 and filled symbols for $\lambda=30$ & 50. (See figure 4 for explanation of tuft location numbers.) Note that the solid line (—) is comparison data from Hill & Peterson³ for the case without Gurney flap.